Counterfactual Generation Under Confounding

Abbavaram Gowtham Reddy*
IIT Hyderabad, India
cs19resch11002@iith.ac.in

Saloni Dash*
Mircosoft Research Bengaluru, India
salonidash77@gmail.com

Amit Sharma
Microsoft Research Bengaluru, India
amshar@microsoft.com

Vineeth N Balasubramanian
IIT Hyderabad, India
vineethnb@iith.ac.in

Abstract

A machine learning model, under the influence of observed or unobserved confounders in the training data, can learn spurious correlations and fail to generalize when deployed. For image classifiers, augmenting a training dataset using counterfactual examples has been empirically shown to break spurious correlations. However, the counterfactual generation task itself becomes more difficult as the level of confounding increases. Existing methods for counterfactual generation under confounding consider a fixed set of interventions (e.g., texture, rotation) and are not flexible enough to capture diverse data-generating processes. We formally characterize the adverse effects of confounding on any downstream tasks and show that the correlation between generative factors can be used to quantitatively measure confounding. To minimize such correlation, we propose a counterfactual generation method that learns to modify the value of any attribute in an image and generate new images. Our method is computationally efficient, simple to implement, and works well for any number of generative factors and confounding variables. Our experimental results on both synthetic (MNIST variants) and real-world (CelebA) datasets show the usefulness of our approach.

1 Introduction

A confounder is a variable that causally influences two or more variables that are not necessarily directly causally dependent [26]. Often, the presence of confounders in a data-generating process is the reason for spurious correlations among variables in the observational data. The bias caused by such confounders is inevitable in observational data, making it challenging to identify invariant features representative of a target variable [33, 24, 39]. Removing the effects of confounding in trained machine learning models has shown to be helpful in various applications such as disentanglement, domain generalization, counterfactual generation, algorithmic fairness, etc. [35, 19, 2, 45, 42, 34, 11, 6, 32, 9]. Recent years have seen a few efforts to handle the spurious correlations caused by confounding effects in observational data [36, 34, 11, 32]. However, these methods either make strong assumptions on the underlying causal generative process or require strong supervision. In this paper, we study the adversarial effect of confounding in observational data on a classifier's performance and propose a mechanism to marginalize such effects by counterfactual data augmentation.

The causal generative processes considered throughout this paper are shown in Figure 1(a). We assume that a set of generative factors (attributes) $Z_1, Z_2, \dots, Z_n$ (e.g., *background, shape, texture*) and a label Y (e.g., *cow*) *cause* a real-world observation X (e.g., an image of a cow in a particular background) through an unknown causal mechanism g [28]. To study the effects of confounding, we consider $Y, Z_1, Z_2, \dots, Z_n$ to be confounded by a set of confounding variables $C_1, \dots, C_m$

*Equal contribution

NeurIPS 2022Workshop on Causal Machine Learning for Real-World Impact (CML4Impact 2022).

(e.g., certain breeds of *cows* appear only in certain *shapes* or *colors* and appear only in certain *countries*). Such causal generative processes have been considered earlier for other kinds of tasks such as disentanglement [35, 37, 32].

A related recent effort by [34] proposes Counterfactual Generative Networks (CGN) to address this problem using a data augmentation approach. This work assumes each image to be composed of three Independent Causal Mechanisms (ICMs) [29] responsible for three fixed factors of variations: *shape, texture*, and *background* (as represented by Z_1, Z_2, and Z_3 in Figure 1(b). This work then trains a generative model that learns three ICMs for *shape, texture*, and *background* separately, and combines them in a deterministic fashion to generate observations. However, fixing the architecture to specific number and types of mechanisms (*shape, texture, background*) is not generalizable, and may not directly be applicable to settings where the number of underlying generative factors is unknown. It is also computationally expensive to train different generative models for each aspect of an image such as *texture*, *shape* or *background*.

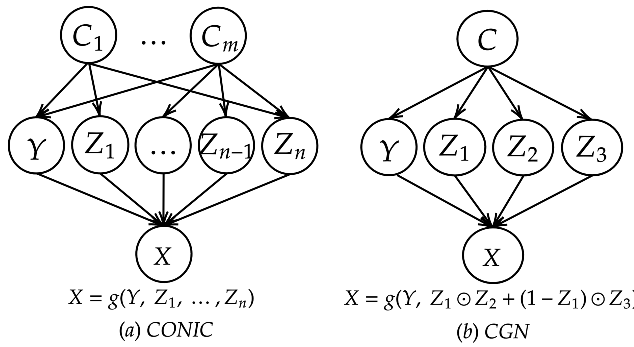

Figure 1: *(a)* causal data generating process considered in this paper (CONIC = Ours); *(b)* causal data generating process considered in CGN [34].

In this work, we begin with quantifying confounding in observational data that is generated by an underlying causal graph of the form shown in Figure 1(a). We then provide a counterfactual data augmentation methodology called CONIC (COunterfactual geNeratIon under Confounding). We hypothesize that the counterfactual images generated using the proposed CONIC method provide a mechanism to marginalize the causal mechanisms responsible for spurious correlations (i.e., causal arrows from C_i to Z_j for some i, j). We take a generative modeling approach and propose a neural network architecture based on conditional CycleGAN [46] to generate counterfactual images. Our contributions include:

- We formally quantify confounding in causal generative processes of the form in Fig 1(a), and study the relationship between correlation and confounding between any pair of generative factors.
- We present a counterfactual data augmentation methodology to generate counterfactual instances of observed data, that can work even under highly confounded data ($\sim 95\%$ confounding) and provides a mechanism to marginalize the causal mechanisms responsible for confounding.
- We modify conditional CycleGAN to improve the quality of generated counterfactuals. Our method is computationally efficient and easy to implement.
- Following previous work, we perform extensive experiments on well-known benchmarks – three MNIST variants and CelebA datasets – to showcase the usefulness of our proposed methodology in improving the accuracy of a downstream classifier.

2 Related Work

Counterfactual Inference: [27], in his seminal text on causality, provided a three-step procedure for generation of a counterfactual data instance, given an observed instance: (i) *Abduction:* abduct/recover the values of exogenous noise variables; (ii) *Action:* perform the required intervention; and (iii) *Prediction:* generate the counterfactual instance. One however needs access to the underlying structural causal model (SCM) to perform the above steps for counterfactual generation. Since real-world data do not come with an underlying SCM, many recent efforts have focused on modeling the underlying causal mechanisms generating data under various assumptions [21, 18, 7, 47, 30, 41, 3, 25].

Generating Counterfactuals by Learning ICMs: In a more recent effort, assuming any real-world image is generated with three independent causal mechanisms for *shape, texture, background*, and a *composition* mechanism of the first three, [34] developed Counterfactual Generative Networks (CGN) that generate counterfactual images of a given image. CGN trains three Generative Adversarial Networks (GANs) [13] to learn *shape, texture, background* mechanisms and combine these three mechanisms using a composition mechanism g as $g(shape, texture, background) = shape \odot$

$texture + (1 - shape) \odot background$ where $\odot$ is the Hadamard product. However, such deterministic nature of the architecture is not generalizable to the case where the number of underlying generative factors are unknown and it is computationally infeasible to train generative models for specific aspect of an image such as texture/background.

Disentanglement and Data Augmentation: The spurious correlations among generative factors have been considered in disentanglement [10, 38]. The general idea in these efforts is to separate the causal predictive features from non-causal/spurious predictive features to predict an outcome. Our goal is different from disentanglement, and we focus on the performance of a downstream classifier instead of separating the sources of generative factors. Traditional data augmentation methods such as rotation, scaling, corruption, etc. [15, 8, 44, 43] do not consider the causal generative process and hence they can not remove the confounding in the images via data augmentation.

A similar effort to our paper is by [11] who use CycleGAN to generate counterfactual data points. However, they focus on the performance of a subgroup (a subset of data with specific properties) which is different from our goal of controlling confounding in the entire dataset. Another recent work by [39] considers spurious correlations among generative factors and uses CycleGAN to generate counterfactual images. Compared to these efforts, rather than using CycleGAN directly, we propose a CycleGAN-based architecture that is optimized for *controlled* generation using contrastive losses.

3 Information Theoretic Measure of Confounding

Background and Problem Formulation: Let $\{Z_1, Z_2, \ldots, Z_n\}$ be a set of random variables denoting the generative factors of an observed data point X, and Y be the label of the observation X. Each generative factor Z_i (e.g., *color*) can take on a value form a discrete set of values $\{z_i^1, \ldots, z_i^d\}$ (e.g., *red, green* etc.). Let the set $S = \{Y, Z_1, \ldots, Z_n\}$ generates N real-world observations $\{X_i\}_{i=1}^N$ through an unknown causal mechanism g (Fig. 1). Each X_i can be thought of as an observation generated using the causal mechanism g with certain intervention on the variables in the set S. Variables in S may potentially be confounded by a set of confounders $C = \{C_1, \ldots, C_m\}$ that denote real-world confounding such as selection bias. Let $\mathcal{D}$ be the dataset of real-world observations along with corresponding values taken by $\{Y, Z_1, \ldots, Z_n\}$. From a causal effect perspective, each variable in S has a direct causal influence on the observation X (e.g., the causal edge $Z_i \rightarrow X$) and also has non-causal influence on X via the confounding variables $C_1, \ldots, C_m$ (e.g., $Z_i \leftarrow C_j \rightarrow Z_k \rightarrow X$ for some C_j and Z_k). These paths via the confounding variables, in which there is an incoming arrow to the variables in S, are also referred to as *backdoor paths* [26].

In any downstream application where $\mathcal{D}$ is used to train a model (e.g., classification), it is desirable to minimize or remove the effect of confounding variable to ensure that a model is not exploiting the spurious correlations in the data to arrive at a decision. In this paper, we present a method to remove the effect of such confounding variables using counterfactual data augmentation. We first study the relationship between confounding and the correlation between a pair of generative factors.

Definition 3.1. ***(Directed Information [31, 40]).*** *In a causal directed acyclic graph (DAG) $\mathcal{G} = (\mathcal{V}, \mathcal{E})$, where $\mathcal{V}$ denotes the set of variables and $\mathcal{E}$ denotes the set of directed edges denoting the direction of causal influence among the variables in $\mathcal{V}$, the directed information from a variable $Z_i \in \mathcal{V}$ to another variable $Z_j \in \mathcal{V}$ is denoted by $I(Z_i \rightarrow Z_j)$. It is defined as follows.*

$$I(Z_i \rightarrow Z_j) \coloneqq D_{KL}(p(Z_i|Z_j)||p(Z_i|do(Z_j))|p(Z_j)) \coloneqq \mathbb{E}_{p(Z_i,Z_j)} \log \frac{p(Z_i|Z_j)}{p(Z_i|do(Z_j))} \tag{1}$$

Using Definition 3.1, it is easy to see that the variables Z_i and Z_j are unconfounded if and only if $I(Z_j \rightarrow Z_i) = 0$. Non zero directed information $I(Z_j \rightarrow Z_i)$ entails that, $p(Z_i|Z_j) \neq p(Z_i|do(Z_j))$ and hence the presence of confounding (if there is no confounder, $p(Z_i|Z_j)$ should be equal to $p(Z_i|do(Z_j))$). Also, it is important to note that the directed information is not symmetric (i.e., $I(Z_i \rightarrow Z_j) \neq I(Z_j \rightarrow Z_i)$) [17]. We use this fact in defining the measure of confounding below. Since we need to quantify the notion of *confounding* (as opposed to *no confounding*), we use directed information to quantify *confounding* as defined below.

Definition 3.2. ***(An Information Theoretic Measure of Confounding.)*** *In a causal directed acyclic graph (DAG) $\mathcal{G} = (\mathcal{V}, \mathcal{E})$, where $\mathcal{V}$ denotes the set of variables and $\mathcal{E}$ denotes the set of directed edges denoting the direction of causal influence among the variables in $\mathcal{V}$, the amount of confounding between a pair of variables $Z_i \in \mathcal{V}$ and $Z_j \in \mathcal{V}$ is equal to $I(Z_i \rightarrow Z_j) + I(Z_j \rightarrow Z_i)$.*

Since directed information is not symmetric, we define the measure of confounding to include the directed information from one variable to the other for a given pair of variables Z_i, Z_j. We now relate the quantity $I(Z_i \rightarrow Z_j) + I(Z_j \rightarrow Z_i)$ with the correlation between generative factors so that it is easy to quantify the amount of confounding in observational data. Before that, we present the following proposition which will be used in the proof of the subsequent proposition.

Proposition 3.1. *In causal processes of the form 1(a), $p(Z_i|do(Z_j))$ is equal to $p(Z_i)$.*

Proposition 3.2. *For causal generative processes of the form 1(a), the correlation between a pair of generative factors (Z_i, Z_j) is proportional to the amount of confounding between Z_i and Z_j.*

Proofs are provided in Appendix. Using the connection between the confounding and correlation in causal graph 1(a), our objective is to generate counterfactual data such that the resultant dataset after augmentation has no spurious correlations between generative factors. If we observe spurious correlation between two generative factors Z_i, Z_j when they take on the values z_i and z_j respectively, generating counterfactual instances w.r.t. Z_j with the intervention $do(Z_j = z'_j)$ and adding the counterfactual instances to original data breaks the correlation between Z_i, Z_j. We now present our algorithm to generate counterfactual images in a systematic manner.

4 CONIC: Methodology

We propose a way to systematically generate counterfactual data that can marginalize the effect of any confounding edge $C_i \rightarrow Z_j$ in Fig. 1 (a) as explained below.

Removing The Confounding Effect of $C_i \rightarrow Z_j$: In the causal graphs of the form 1(a), for paths of the form $Z_j \leftarrow C_i \rightarrow Z_l$, we call the edges $C_i \rightarrow Z_j$ and $C_i \rightarrow Z_l$ as confounding edges since together, their existence is the reason for confounding in the data. Also, let (z_j^p, z_l^q) is one pair of attribute values taken by the variable pair (Z_j, Z_l) under extreme confounding (e.g., in the training set of colored MNIST dataset, correlation coefficient of 0.99 between *color* and *digit* is observed such that whenever *color* is *red*, *digit* is 7 etc.). To remove the effect of the confounding edge $C_i \rightarrow Z_j$ w.r.t. the another confounding edge $C_i \rightarrow Z_l$ (recall that confounding between Z_j, Z_l is present if and only if there exists a pair of causal arrows $C_i \rightarrow Z_j$ and $C_i \rightarrow Z_l$ for some i; due to this reason we consider the confounding effect of the confounding edge $C_i \rightarrow Z_j$ w.r.t. another confounding edge $C_i \rightarrow Z_l$), we consider two subsets T_1, T_2 of the observational data $\mathcal{D}$ which are constructed as follows. T_1 consists of the set of instances for which $Z_j \neq z_j^p$ and $Z_l = z_l^q$, T_2 consists of the set of instances for which $Z_j = z_j^p$ and $Z_l = z_l^q$. The size of T_1 is usually much smaller than the size of T_2 because of high correlation between Z_j and Z_l (e.g., there are more *red* 7's than *non-red* 7's).

Now, we learn a mapping $\mathcal{M}$ from the set T_1 to the set T_2 that changes the attribute Z_j while fixing the value of Z_l at z_l^q. That is, for any given instance $X \in T_1$, for which $Z_j \neq z_j^p$, $\mathcal{M}$ maps X to a different instance X' in which the value of the generative factor Z_j is changed to z_j^p (e.g., $\mathcal{M}$ takes *red* 9 as input and returns *red* 7 as output). This mapping $\mathcal{M}$ can be thought of as a function performing the 3-step counterfactual inference: learning the underlying generative factors, performing the intervention $do(Z_j = z_j^p)$ and then generating the counterfactual instance X'. Now, given an instance X for which $Z_j \neq z_j^p$ and $Z_l \neq z_l^q$, using $\mathcal{M}$, we can generate counterfactual instance X' in which $Z_j = z_j^p$ and $Z_l \neq z_l^q$. These counterfactual instances, when augmented with the original observed dataset $\mathcal{D}$, removes the effect of the confounding edge $C_i \rightarrow Z_j$ w.r.t. the edge $C_i \rightarrow Z_l$. That is, the counterfactual instances, when augmented with original data, breaks the correlation between Z_j and Z_l. This process can now be repeated systematically for each confounding edge to generate

Algorithm 1: Counterfactual Generation to Remove the Effect of Confounding Edge $C_i \rightarrow Z_j$

Result: Counterfactual images that remove the confounding effect caused by the edge $C_i \rightarrow Z_j$
Input: $\mathcal{D} = \{X_i\}_{i=1}^N$,
$Nodes = \{Z_l | C_i \rightarrow Z_j \& C_i \rightarrow Z_l\}$
Initialize: $cf\_images = []$
for *each* $Z_l \in Nodes$ **do**
  $T_1 = \{X \in \mathcal{D} | Z_j \neq z_j^p \& Z_l = z_l^q\}$
  $T_2 = \{X \in \mathcal{D} | Z_j = z_j^p \& Z_l = z_l^q\}$
  $\mathcal{M} = conditionalCycleGAN(T_1, T_2)$
  $Factual\_Imgs = \{X \in \mathcal{D} | Z_j \neq z_j^p \& Z_l \neq z_l^q\}$
  $Counterfactuals = \mathcal{M}(Factual\_Imgs)$
  $cf\_images.append(Counterfactuals)$
end
return cf_images

counterfactual instances that remove the spurious correlations. The overall procedure to generate counterfactual instances is summarized in Algorithm 1.

Earlier works use CycleGAN to generate counterfactual images that differ from original image by a single attribute/feature [39, 11]. Given two domains/sets of images that differ w.r.t. only one generative factor Z_j, a CycleGAN can learn to translate between the two domains by changing the attribute value of Z_j. In this case, one can think of CycleGAN as a function performing the required intervention Z_j and generating counterfactual instance without modeling the underlying causal process. Concretely, CycleGAN is an architecture used to perform unsupervised domain translation using unpaired images. In a CycleGAN, a generator G_1 first transforms a given image X from a domain/set T_1 into X' so that X' appears to come from another domain/set T_2 such that certain features from input X are preserved in the output X'. A discriminator D_{T_2} then classifies whether the translated image X' is original (i.e., sampled from T_2) or fake (i.e., generated by G_1). A second generator G_2 transforms the image X' back to original image X to ensure that G_1 is using the contents of X to generate X'. The same procedure is repeated to translate images from domain T_2 into domain T_1. The loss function of CycleGAN can be written as $\mathcal{L}_{CycleGAN} = \mathcal{L}_{GAN}(G_1, D_{T_2}, X, X') + \mathcal{L}_{GAN}(G_2, D_{T_1}, X', X) + \mathcal{L}_{cycle}(G_1, G_2)$ Where $\mathcal{L}_{GAN}$ is simple Generative Adversarial Network (GAN) [12] loss and $\mathcal{L}_{cycle}$ is cycle consistency loss measuring how well the output of G_2 is matching with the original input X. For example, $\mathcal{L}_{cycle}(G_1, G_2) = \mathbb{E}_{X\sim\mathcal{D}}[||G_2(G_1(X)) - X||_1]$ can ensure that $G_2(G_1(X)) = X$. We use conditional variant of CycleGAN to leverage the supervision in terms of attribute values. For each generator, along with input, we also feed a desired target attribute as shown in the Figure 2.

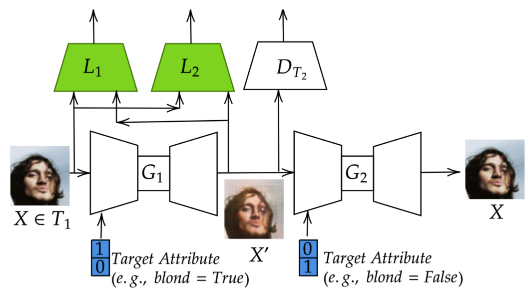

Figure 2: Architecture of the proposed modified conditional CycleGAN. Pre-trained modules are shown in green color and target attribute is shown in blue color. For simplicity, we only show one pass of conditional CycleGAN (translation from T_1 to T_2) in this figure.

To improve the quality of counterfactual images generated by conditional CycleGAN under extreme confounding, we propose a modification to conditional CycleGAN as detailed below. As discussed earlier, X', the output of G_1, can be thought of as a counterfactual image of X. When changing the feature Z_j of X, we keep the feature Z_l fixed. That is, the representation for Z_j in both X and X' should be different and the representation for Z_l in both X and X' should be same. To ensure this, as shown in Figure 2, along with two generators G_1, G_2 and a discriminator D_{T_2} that are part of conditional CycleGAN, we add two pre-trained discriminators L_1, L_2 (shown in green color in Fig. 2). L_1 takes two images X, X' as input and returns high penalty if the representation of Z_j is similar in X, X' and small penalty otherwise. L_2 takes two images X, X' as input and returns high penalty if the representation of Z_l is different and small penalty otherwise. Thus, our overall objective to generate good quality counterfactual images is to train the modified conditional CycleGAN by minimizing the following objective.

$$\begin{aligned}\mathcal{L}_{conic} = \mathcal{L}_{CycleGAN} - \mathcal{L}_{con}(L_1(X), L_1(G_1(X))) + \mathcal{L}_{con}(L_2(X), L_2(G_1(X))) \\ - \mathcal{L}_{con}(L_1(X'), L_1(G_2(X'))) + \mathcal{L}_{con}(L_2(X'), L_2(G_2(X')))\end{aligned} \quad (2)$$

Where $\mathcal{L}_{con}$ is the contrastive loss [14]. For a pair of images (X, X'), $\mathcal{L}_{con}$ defined $\mathcal{L}_{con}(X, X') = AD^2 + (1 - A)\max(\epsilon - D, 0)^2$ Where $A = 1$ if X, X' belong to same class (or have same attribute values), $A = 0$ if X, X' belong to different classes (or have different attribute values). D is the distance between the representations of X, X' (e.g., Euclidean distance). ϵ is the margin of error allowed between two representations of the images of different classes. L_1 and L_2 are pre-trained models and the parameters of L_1 and L_2 are fixed. That is, the loss values returned by $\mathcal{L}_{contrastive}$ are only used to update the trainable parameters of conditional CycleGAN.

A Downstream Task - Image Classification: To measure the goodness of counterfactual generation, we consider the classification task on the unconfounded test set as a downstream task. Let $\mathcal{D}^{aug} = \{(X_i, Y_i)\}_{i=1}^{M}$ be the augmented dataset of original data $\mathcal{D}$ and corresponding counterfactual data points. Using $\mathcal{D}^{aug}$, we minimize $\mathcal{L}_{aug} := \mathbb{E}_{(X,y)\sim\mathcal{D}^{aug}}[l(f_\theta(X), y)]$. Where l is cross entropy loss.

To further improve the performance of a classifier using $\mathcal{D}^{aug}$, for each pair of images X_i, X_j we minimize $\mathcal{L}_{con}(X_i, X_j)$ on the logits in the final layer. Now, the final objective to optimize for classification task is to minimize$\mathcal{L} = \mathcal{L}_{aug} + \lambda \mathbb{E}_{(X_i,X_j)\sim(\mathcal{D}^{aug}\times\mathcal{D}^{aug})}[\mathcal{L}_{contrastive}(X_i, X_j)]$ Where $\lambda > 0$ is a regularization hyperparameter.

5 Experiments and Results

We now present the experimental results on both synthetic (MNIST variants) and real world (CelebA) datasets. Having access to the ground truth generative factors (i.e., $Z_1, \ldots, Z_n$), we artificially create confounding in the training data and we leave test data to be unconfounded (i.e., no correlation among generative factors). We compare CONIC with various baselines including Empirical Risk Minimizer (ERM), Conditional GAN (CGAN) [12], Conditional VAE (CVAE) [20], Conditional-β-VAE (C-β-VAE) [16], AugMix [15], CutMix [43], Invariant Risk Minimization (IRM) [1], and Counterfactual Generative Networks (CGN) [34].

MNIST Variants: We construct the following three synthetic datasets based on MNIST dataset [22] and its colored, texture, and morpho (where the digit thickness is controlled; Fig. 3) variants [1, 4, 34]: (i) colored morpho MNIST (CM-MNIST), (ii) double colored morpho MNIST (DCM-MNIST), and (iii) wildlife morpho MNIST (WLM-MNIST). We consider extreme confounding among generative factors as explained below. For the experimental results shown in Table 1, in the training set of CM-MNIST dataset, the correlation coefficient between digit label and digit color $r(label, color)$ is 0.95 and the digits from 0 to 4 are thin and digits from 5 to 9 are thick (see Figure 3). That is, $r(label, thin) = 1$ if the digit is in [0,1,2,3,4] else $r(label, thick) = 1$. In the training set of DCM-MNIST dataset, digit label, digit color, and background color jointly take a fixed set of values 95% of the time. That is, $r(label, color) = r(color, background) = r(label, background) = 0.95$ and the digits from 0 to 4 are thin and digits from 5 to 9 are thick. In the training set of WLM-MNIST dataset digit shape, digit texture, and background texture jointly take a fixed set of attribute values 95% of the time and the digits from 0 to 4 are thin and digits from 5 to 9 are thick. Table 1 shows the results in which CONIC outperforms all the baselines. See Appendix for comparison of augmented images by various baselines. Coninc uses only 10000, 15000, 15000 counterfactual images in CM-MNIST, DCM-MNIST, and WLM-MNIST experiments respectively to get improved performance.

Model	CM-MNIST	DCM-MNIST	WLM-MNIST	CelebA
ERM	46.41± 0.81%	43.31 ± 2.30%	28.28 ± 0.70%	70.64 ± 6.93%
CGAN	41.86 ± 1.79%	30.66 ± 3.86%	17.50 ± 0.85%	70.99 ± 2.35%
CVAE	49.58 ± 1.50%	41.99 ± 1.10%	34.19 ± 1.58%	71.50 ± 1.82%
C-β-VAE	51.22 ± 1.00%	51.58 ± 2.36%	33.90 ± 1.87%	74.29 ± 0.65%
AugMix	47.36 ± 0.01%	44.85 ± 0.02%	26.30 ± 1.30%	71.93 ± 4.64%
CutMix	20.44 ± 1.22%	23.10 ± 2.98%	12.08 ± 1.59%	73.66 ± 0.76%
IRM	55.25 ± 0.89%	49.71 ± 0.71%	50.26 ± 0.48%	72.30 ± 2.71%
CGN	42.15 ± 3.89%	47.50 ± 2.18%	43.84 ± 0.25%	69.25 ± 0.29%
CONIC	**65.57 ± 0.34%**	**92.41 ± 0.26%**	**77.72± 1.00%**	**79.56 ± 1.28%**

Table 1: Test set accuracy results on MNIST variants and CelebA

CelebA: Unlike MNIST variants, CelebA [23] dataset implicitly contains confounding (e.g., the percentage of *males* with *blond hair* is different from the percentage of *females* with *blond hair*, in addition to the difference in the total number of *males* and *females* in the dataset). In this experiment, we consider the performance of a classifier trained on the augmented data that predicts hair color given an image. Our test set is the set of *males* with *blond hair*. We train models on the train set and test the performance on the set of *males* with *blond hair*. Since the number of *males* with blond hair is very low in the dataset (approximately 4% of *males* have *blond hair*), we show that the augmenting the train set with only 10000 images of *males* with *blond hair* improves the performance over baselines (see Table 1) whereas other baselines require more than 50000 augmented images to get minor improvement over ERM. Given a *male* image with *non-blond hair*, CONIC generates the counterfactual image with *blond hair* without changing the *male* attribute (see Appendix for sample counterfactual images). We also note that the deterministic models such as CGN fail when they are applied to a different task where the number and type of generative factors are not fixed and are difficult to separate (e.g., CelebA). CGN results in table 1 are obtained with only 1000 counterfactual images as augmented data points. When we increase the number of counterfactual instances, performance of CGN reduces further.

6 Conclusions

We studied the adverse effects of confounding in observational data on the performance of a classifier. We showed the relationship between confounding and correlation in the causal processes considered, and we proposed a methodology to remove the correlation between the target variable and generative factors that works even when the dataset is highly confounded. Specifically, we proposed a counterfactual data augmentation method that systematically removes the confounding effect rather than addressing the confounding problem through random augmentations. Using the generated counterfactuals leads to substantial increase in a downstream classifier's accuracy. That said, we observed that the counterfactual quality can still be improved, which will be interesting future work.

References

[1] Martin Arjovsky, Léon Bottou, Ishaan Gulrajani, and David Lopez-Paz. Invariant risk minimization, 2019.

[2] Yuval Atzmon, Felix Kreuk, Uri Shalit, and Gal Chechik. A causal view of compositional zero-shot recognition. In *NeurIPS*, 2020.

[3] Ioana Bica, James Jordon, and Mihaela van der Schaar. Estimating the effects of continuous-valued interventions using generative adversarial networks. In H. Larochelle, M. Ranzato, R. Hadsell, M. F. Balcan, and H. Lin, editors, *NeurIPS*, volume 33, pages 16434–16445. Curran Associates, Inc., 2020.

[4] Daniel C. Castro, Jeremy Tan, Bernhard Kainz, Ender Konukoglu, and Ben Glocker. Morpho-MNIST: Quantitative assessment and diagnostics for representation learning. *JMLR*, 20(178), 2019.

[5] Yunjey Choi, Minje Choi, Munyoung Kim, Jung-Woo Ha, Sunghun Kim, and Jaegul Choo. Stargan: Unified generative adversarial networks for multi-domain image-to-image translation. In *CVPR*, 2018.

[6] Saloni Dash, Vineeth N Balasubramanian, and Amit Sharma. Evaluating and mitigating bias in image classifiers: A causal perspective using counterfactuals. In *WACV*, 2022.

[7] Emily Denton, Ben Hutchinson, Margaret Mitchell, and Timnit Gebru. Detecting bias with generative counterfactual face attribute augmentation, 2019.

[8] Terrance Devries and Graham W. Taylor. Improved regularization of convolutional neural networks with cutout. *ArXiv*, abs/1708.04552, 2017.

[9] Richard Dinga, Lianne Schmaal, Brenda W.J.H. Penninx, Dick J. Veltman, and Andre F. Marquand. Controlling for effects of confounding variables on machine learning predictions. *bioRxiv*, 2020.

[10] Christina M Funke, Paul Vicol, Kuan-Chieh Wang, Matthias Kuemmerer, Richard Zemel, and Matthias Bethge. Disentanglement and generalization under correlation shifts. In *ICLR2022 Workshop on the Elements of Reasoning: Objects, Structure and Causality*, 2022.

[11] Karan Goel, Albert Gu, Yixuan Li, and Christopher Re. Model patching: Closing the subgroup performance gap with data augmentation. In *ICLR*, 2021.

[12] Ian J. Goodfellow, Jean Pouget-Abadie, Mehdi Mirza, Bing Xu, David Warde-Farley, Sherjil Ozair, Aaron Courville, and Yoshua Bengio. Generative adversarial networks, 2014.

[13] Ian J. Goodfellow, Jean Pouget-Abadie, Mehdi Mirza, Bing Xu, David Warde-Farley, Sherjil Ozair, Aaron C. Courville, and Yoshua Bengio. Generative adversarial nets. In *NIPS*, pages 2672–2680, 2014.

[14] R. Hadsell, S. Chopra, and Y. LeCun. Dimensionality reduction by learning an invariant mapping. In *CVPR*, 2006.

[15] Dan Hendrycks, Norman Mu, Ekin Dogus Cubuk, Barret Zoph, Justin Gilmer, and Balaji Lakshminarayanan. Augmix: A simple method to improve robustness and uncertainty under data shift. In *ICLR*, 2020.

[16] Irina Higgins, Loic Matthey, Arka Pal, Christopher Burgess, Xavier Glorot, Matthew Botvinick, Shakir Mohamed, and Alexander Lerchner. beta-VAE: Learning basic visual concepts with a constrained variational framework. In *International Conference on Learning Representations*, 2017.

[17] Jiantao Jiao, Haim H Permuter, Lei Zhao, Young-Han Kim, and Tsachy Weissman. Universal estimation of directed information. *IEEE Transactions on Information Theory*, 59(10):6220–6242, 2013.

[18] Jungseock Joo and Kimmo Kärkkäinen. Gender slopes: Counterfactual fairness for computer vision models by attribute manipulation. In *Proceedings of the 2nd International Workshop on Fairness, Accountability, Transparency and Ethics in Multimedia*, FATE/MM '20, page 1–5, New York, NY, USA, 2020. Association for Computing Machinery.

[19] Niki Kilbertus, Philip J Ball, Matt J Kusner, Adrian Weller, and Ricardo Silva. The sensitivity of counterfactual fairness to unmeasured confounding. In *UAI*, 2020.

[20] Diederik P Kingma and Max Welling. Auto-encoding variational bayes, 2013.

[21] Matt J Kusner, Joshua Loftus, Chris Russell, and Ricardo Silva. Counterfactual fairness. In I. Guyon, U. V. Luxburg, S. Bengio, H. Wallach, R. Fergus, S. Vishwanathan, and R. Garnett, editors, *NeurIPS*, volume 30. Curran Associates, Inc., 2017.

[22] Y. Lecun, L. Bottou, Y. Bengio, and P. Haffner. Gradient-based learning applied to document recognition. *Proceedings of the IEEE*, 86(11):2278–2324, 1998.

[23] Ziwei Liu, Ping Luo, Xiaogang Wang, and Xiaoou Tang. Deep learning face attributes in the wild. In *ICCV*, 2015.

[24] Nicolai Meinshausen and Peter Bühlmann. Maximin effects in inhomogeneous large-scale data. *The Annals of Statistics*, 43(4):1801 – 1830, 2015.

[25] Nick Pawlowski, Daniel Coelho de Castro, and Ben Glocker. Deep structural causal models for tractable counterfactual inference. In H. Larochelle, M. Ranzato, R. Hadsell, M. F. Balcan, and H. Lin, editors, *NeurIPS*, volume 33, pages 857–869. Curran Associates, Inc., 2020.

[26] Judea Pearl. Direct and indirect effects. In *UAI*, pages 411–420, 2001.

[27] Judea Pearl. *Causality*. Cambridge university press, 2009.

[28] J. Peters, D. Janzing, and B. Scholkopf. *Elements of Causal Inference: Foundations and Learning Algorithms*. Adaptive Computation and Machine Learning series. MIT Press, 2017.

[29] J. Peters, D. Janzing, and B. Schölkopf. *Elements of Causal Inference: Foundations and Learning Algorithms*. MIT Press, Cambridge, MA, USA, 2017.

[30] Silviu Pitis, Elliot Creager, and Animesh Garg. Counterfactual data augmentation using locally factored dynamics. In H. Larochelle, M. Ranzato, R. Hadsell, M. F. Balcan, and H. Lin, editors, *NeurIPS*, volume 33, pages 3976–3990. Curran Associates, Inc., 2020.

[31] Maxim Raginsky. Directed information and pearl's causal calculus. In *2011 49th Annual Allerton Conference on Communication, Control, and Computing (Allerton)*, pages 958–965, 2011.

[32] Abbavaram Gowtham Reddy, Benin L Godfrey, and Vineeth N Balasubramanian. On causally disentangled representations. In *AAAI*, 2022.

[33] Dominik Rothenhäusler, Nicolai Meinshausen, Peter Bühlmann, Jonas Peters, et al. Anchor regression: Heterogeneous data meet causality. *Journal of the Royal Statistical Society Series B*, 83(2):215–246, 2021.

[34] Axel Sauer and Andreas Geiger. Counterfactual generative networks. In *ICLR*, 2021.

[35] Raphael Suter, Djordje Miladinovic, Bernhard Schölkopf, and Stefan Bauer. Robustly disentangled causal mechanisms: Validating deep representations for interventional robustness. In *ICML*, 2019.

[36] Frederik Träuble, Elliot Creager, Niki Kilbertus, Francesco Locatello, Andrea Dittadi, Anirudh Goyal, Bernhard Schölkopf, and Stefan Bauer. On disentangled representations learned from correlated data. In *ICML*, 2021.

[37] Julius Von Kügelgen, Yash Sharma, Luigi Gresele, Wieland Brendel, Bernhard Schölkopf, Michel Besserve, and Francesco Locatello. Self-supervised learning with data augmentations provably isolates content from style. *Advances in neural information processing systems*, 34:16451–16467, 2021.

[38] Julius von Kügelgen, Yash Sharma, Luigi Gresele, Wieland Brendel, Bernhard Schölkopf, Michel Besserve, and Francesco Locatello. Self-supervised learning with data augmentations provably isolates content from style. In *NeurIPS*, 2021.

[39] Ruoyu Wang, Mingyang Yi, Zhitang Chen, and Shengyu Zhu. Out-of-distribution generalization with causal invariant transformations. In *CVPR*, 2022.

[40] Aleksander Wieczorek and Volker Roth. Information theoretic causal effect quantification. *Entropy*, 21(10), 2019.

[41] Jinsung Yoon, James Jordon, and Mihaela van der Schaar. GANITE: estimation of individualized treatment effects using generative adversarial nets. In *6th ICLR, ICLR 2018, Vancouver, BC, Canada, April 30 - May 3, 2018, Conference Track Proceedings*. OpenReview.net, 2018.

[42] Zhongqi Yue, Tan Wang, Qianru Sun, Xian-Sheng Hua, and Hanwang Zhang. Counterfactual zero-shot and open-set visual recognition. In *CVPR*, 2021.

[43] Sangdoo Yun, Dongyoon Han, Sanghyuk Chun, Seong Joon Oh, Youngjoon Yoo, and Junsuk Choe. Cutmix: Regularization strategy to train strong classifiers with localizable features. In *ICCV*, pages 6022–6031, 2019.

[44] Hongyi Zhang, Moustapha Cisse, Yann N. Dauphin, and David Lopez-Paz. mixup: Beyond empirical risk minimization. In *ICLR*, 2018.

[45] Qingyu Zhao, Ehsan Adeli, and Kilian M Pohl. Training confounder-free deep learning models for medical applications. *Nature communications*, 11(1):1–9, 2020.

[46] Jun-Yan Zhu, Taesung Park, Phillip Isola, and Alexei A. Efros. Unpaired image-to-image translation using cycle-consistent adversarial networks. In *ICCV*, 2017.

[47] Ran Zmigrod, Sabrina J. Mielke, Hanna Wallach, and Ryan Cotterell. Counterfactual data augmentation for mitigating gender stereotypes in languages with rich morphology, 2019.

Appendix

A Proof of Propositions

Proposition 3.1. *In causal processes of the form 1(a), $p(Z_i|do(Z_j))$ is equal to $p(Z_i)$.*

Proof. In causal processes of the form 1(a), let C' denote the set of all confounding variables that are part of some backdoor path from Z_i to Z_j. That is $C' = \{C|Z_i \leftarrow C \rightarrow Z_j\}$ for some i, j. Then we can evaluate the quantity $p(Z_i|do(Z_j))$ as

$$p(Z_i|do(Z_j)) = \sum_{C'} p(Z_i|Z_j, C')p(C') = \sum_{C'} p(Z_i|C')p(C') = \sum_{C'} p(Z_i, C') = p(Z_i)$$

Where the first equality is because of the adjustment formula [26] and the second equality is because of the fact that Y is a collider in causal graph 1(a) and hence conditioned on C', Z_i is independent of Z_j. □

Proposition 3.2. *For causal generative processes of the form 1(a), the correlation between a pair of generative factors (Z_i, Z_j) is proportional to the amount of confounding between Z_i and Z_j.*

Proof. Expanding the quantity $I(Z_i \rightarrow Z_j) + I(Z_j \rightarrow Z_i)$, we get the following,

$$\begin{aligned}
I(Z_i \rightarrow Z_j) + I(Z_j \rightarrow Z_i) &= \mathbb{E}_{Z_i,Z_j}\left[\log(\frac{p(Z_i|Z_j)}{p(Z_i|do(Z_j))})\right] + \mathbb{E}_{Z_i,Z_j}\left[\log(\frac{p(Z_j|Z_i)}{p(Z_j|do(Z_i))})\right] \\
&= \mathbb{E}_{Z_i,Z_j}\left[\log(\frac{p(Z_i|Z_j)p(Z_j|Z_i)}{p(Z_i|do(Z_j))p(Z_j|do(Z_i))})\right] = \mathbb{E}_{Z_i,Z_j}\left[\log(\frac{p(Z_i|Z_j)p(Z_j|Z_i)}{p(Z_i)p(Z_j)})\right] \\
&= \mathbb{E}_{Z_i,Z_j}\left[\log(\frac{p(Z_i|Z_j)p(Z_j)p(Z_j|Z_i)p(Z_i)}{p(Z_i)p(Z_j)p(Z_i)p(Z_j)})\right] = \mathbb{E}_{Z_i,Z_j}\left[\log(\frac{p(Z_i,Z_j)p(Z_j,Z_i)}{p(Z_i)^2p(Z_j)^2})\right] \\
&= 2 \times \mathbb{E}_{Z_i,Z_j}\left[\log(\frac{p(Z_i,Z_j)}{p(Z_i)p(Z_j)})\right] = 2 \times I(Z_i;Z_j)
\end{aligned} \tag{3}$$

Where the third equality is due to Proposition 3.1. Since non-zero mutual information implies positive correlation, we see that the amount of confounding between Z_i and Z_j is directly proportional to the correlation between Z_i and Z_j. Hence, we use the correlation as a measure of confounding between generative factors in the causal processes of the form 1(a). □

B Time Complexity Analysis:

Apart from its simple methodology, CONIC brings additional advantages in terms of computing time required to train the model that generates counterfactual images. As shown in Table 2, the time required to run our method to generate counterfactual images w.r.t. a generative factor Z_j is significantly less than CGN that learns deterministic causal mechanisms as discussed in Section 2. Even though we used CycleGAN in this work, for the cases where the number of generative factors are more, StarGAN [5] can be used to minimize the time required to learn the mappings from one domain to another domain [39, 11].

Dataset	CONIC	CGN
CM-MNIST	2.76 ± 0.19	103 ± 1.50
DCM-MNIST	2.22 ± 0.01	103 ± 2.04
WLM-MNIST	1.22 ± 0.01	111 ± 2.50

Table 2: Run time (in minutes) of CONIC compared to CGN on MNIST variants

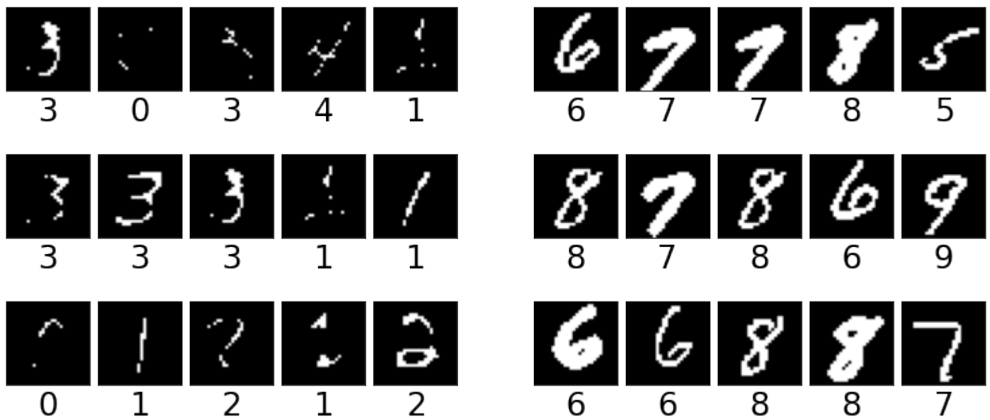

Figure 3: Left: sample thin morpho MNIST images and corresponding labels. Right: Sample thick morpho MNIST images and corresponding labels.

Figure 4: Top: CelebA original images of *males* with *non-blond hair* color. Bottom: Counterfactual images of *males* with *blond hair* generated using Algorithm 1

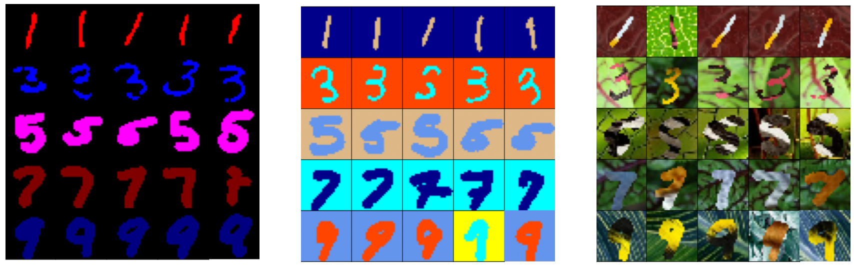

CM-MNIST Samples DCM-MNIST Samples WLM-MNIST Samples

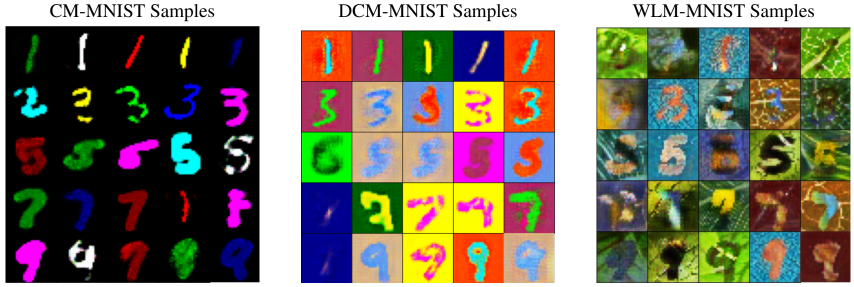

CM-MNIST CONIC DCM-MNIST CONIC WLM-MNIST CONIC

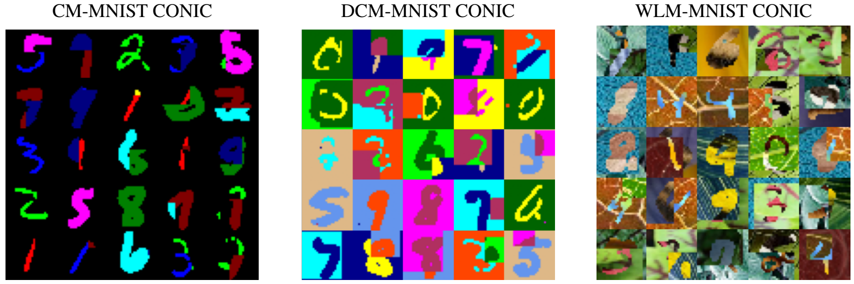

CM-MNIST CUTMix DCM-MNIST CUTMix WLM-MNIST CUTMix

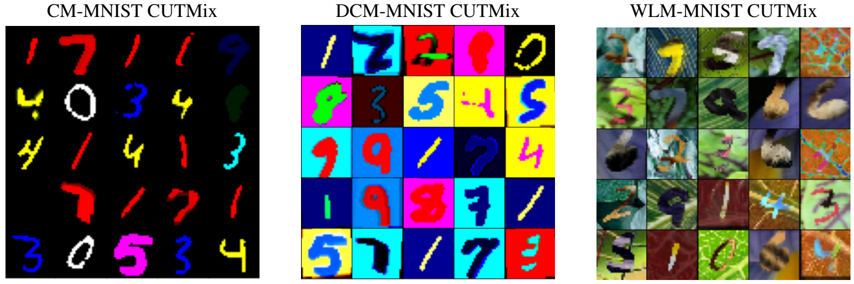

CM-MNIST AUGMix DCM-MNIST AUGMix WLM-MNIST AUGMix

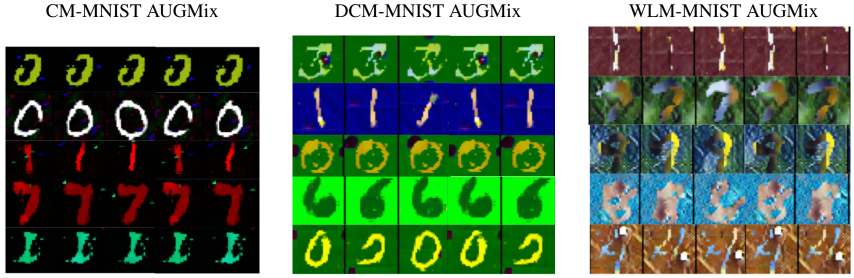

CM-MNIST CGN DCM-MNIST CGN WLM-MNIST CGN

Figure 5: Sample images from MNIST variants and augmented images by various methods.